

**An Emittance Scanner for High-Intensity,
Low-Energy Ion Beams**

by

Jesus Corona

Submitted to the Department of Physics
in partial fulfillment of the requirements for the degree of

Bachelor of Science in Physics

at the

MASSACHUSETTS INSTITUTE OF TECHNOLOGY

June 2018

© Massachusetts Institute of Technology 2018. All rights reserved.

Signature redacted

Author

.....
Department of Physics
May 17, 2018

Signature redacted

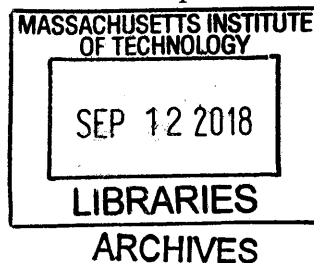
Certified by.

.....
Janet Conrad
Professor of Physics
Thesis Supervisor

Signature redacted

Accepted by

.....
Scott A. Hughes
Interim Associate Department Head, Department of Physics



An Emittance Scanner for High-Intensity, Low-Energy Ion Beams

by

Jesus Corona

Submitted to the Department of Physics
on May 17, 2018, in partial fulfillment of the
requirements for the degree of
Bachelor of Science in Physics

Abstract

My work in this thesis is a contribution toward the IsoDAR experiment, which aims to test the sterile neutrino hypothesis. In the IsoDAR experiment, neutrinos are generated by a 60 MeV proton beam impinging on a ${}^9\text{Be}$ target and diffusing through ${}^7\text{Li}$. This results in ${}^8\text{Li}$ which beta decays, thereby producing an electron-antineutrino beam. To overcome space charge limitations, H_2^+ is accelerated instead of protons. Acceleration is accomplished by a cyclotron, and the beam injected into the cyclotron needs to have a low emittance (a figure of merit for the beam quality). This is where the need for a way to measure our beam's emittance arises. This thesis covers the process of designing, fabricating, assembling, and commissioning an emittance scanner. The main challenges I faced were the high-intensity of the beam and a need for high precision. I designed an emittance scanner using CAD software. Its parts were then machined in MIT's Central Machine Shop and subsequently built and installed into vacuum. As of now, preliminary commissioning of the scanners has begun with a few initial scans already performed. The scanners will soon be further used for better understanding the quality of our beam.

Thesis Supervisor: Janet Conrad

Title: Professor of Physics

Acknowledgments

I am grateful for the mentorship of Postdoctoral Associate Daniel Winklehner throughout my work with MIST-1, in particular for all the guidance and help he has provided. I have learned a lot about being a physicist from him.

I'm also grateful for the assistance and support from Professor Janet Conrad. She has always made working in her group be a welcoming experience.

The work contained in this thesis is of course not solely my own, so I would like to take this moment to highlight and acknowledge the contributions of two other people heavily involved in the project. First, Undergraduate Research Assistant Patrick Bedard who put a lot of work into the initial designing of the emittance scanner, including thermal simulation.

Second, Postbaccalaureate Associate Thomas Wester, who has contributed extensively to the software involved in this project. I had the pleasure of working alongside him for the majority of this work and I am grateful for all the time he has put into it.

Contents

1	Introduction	13
1.1	IsoDAR	14
1.2	Beam Emittance	15
1.3	Measuring Emittance	16
2	Emittance Scanner Hardware	19
2.1	Design Considerations	19
2.1.1	Design Parameters	20
2.1.2	Heat Transfer	23
2.2	Detailed Design	23
3	Controls and Data Acquisition	29
3.1	Hardware	29
3.2	Software	30
4	Preliminary Commissioning	33
4.1	Experimental Setup	33
4.2	Comissioning Results	34
5	Conclusion	39
5.1	Summary	39
5.2	Outlook	39
A	Assembly Design Drawings	41

List of Figures

1-1	A typical trace space ellipse plot	16
2-1	Beam measurement graphic	20
2-2	Visualization of scanner head inner dimensions	22
2-3	Cut-view rendering of the scanner head	22
2-4	Full emittance scanner system rendering	24
2-5	Scanner head exploded view	26
2-6	Rear assembly exploded view	26
3-1	A layout graph of the hardware.	30
4-1	Photo of experimental setup	34
4-2	Raw scan data with no beam	35
4-3	Raw scan data with beam	36
4-4	Analyzed beam emittance scan	37
A-1	Full emittance scanner system assembly	42
A-2	Front plate assembly	43
A-3	Scanner head assembly	44
A-4	Rear collector assembly	45
A-5	Inner telescopic tube assembly	46
A-6	Outer telescopic tube assembly	47
B-1	Vertical emittance scanner installation photo	50
B-2	Horizontal emittance scanner installation photo	51

List of Tables

2.1 Parameters for dimensions of the scanner box 21

4.1 Normalized emittance results 35

Chapter 1

Introduction

In the past decades, neutrino oscillation experiments have seen anomalies that could potentially be explained by introducing a new type of neutrino, the so-called sterile neutrino [8]. In order to decisively test this hypothesis, a new experiment, called IsoDAR (described in Section 1.1) is being developed at MIT. In short, it is an accelerator driven isotropic neutrino source coupled with an underground neutrino detector.

An isotropic neutrino source means only a small percentage of neutrinos produced actually end up entering the detector. This is why a high intensity driver beam is needed, for which I have developed an emittance scanner to be used in the low energy beam transport of this experiment. This scanner is a device that measures the emittance (a figure of merit for the beam quality) of a charged particle beam. In our case, with a multicusp ion source, we will be dealing with maximum beam currents of 20 – 50 mA of H_2^+ . Measuring the emittance of this beam will help us understand how it will behave further on in the beam transport and whether it will meet the demands of the greater goals of IsoDAR.

The structure of this thesis is as follows:

Chapter 1 will cover background and the theory of beam emittance.

Chapter 2 will describe the engineering of the scanner, covering the inspiration for the design, thermal considerations, and the full technical design.

Chapter 3 will discuss the hardware used for operating the scanners and the soft-

ware to control them.

Chapter 4 will cover the experimental setup and first commissioning results.

1.1 IsoDAR

The Isotope Decay-At-Rest (IsoDAR) experiment aims to test the sterile neutrino hypothesis which is the idea that there exists a fourth flavor of neutrino, the sterile neutrino. This would account for various anomalies present in the existing active neutrinos [8]. This is accomplished with measurement of neutrino oscillations through $\bar{\nu}_e$ disappearance via inverse beta decay.

Neutrino production in the IsoDAR experiment relies on a high current, low energy H_2^+ beam which gets stripped to protons before impinging on a ^9Be target, producing neutrons. These neutrons diffuse through a ^7Li sleeve resulting in ^8Li , which then beta-decays and produces a very pure $\bar{\nu}_e$ beam. This anti-neutrino source is then positioned near a kiloton-scale detector such as KamLAND (Kamioka Liquid-scintillator Anti-Neutrino Detector) [1].

The beam that hits the ^9Be target must be 10 mA of protons by design in order to produce enough neutrinos in order to be decisive over three years of running. The beam must also be accelerated to an energy of 60 MeV/amu, which is done using a cyclotron [5]. Instead of 10 mA of protons, we produce 5 mA of H_2^+ due to limitations of the cyclotron and to overcome space charge issues [6].

H_2^+ ion beam production is accomplished with a dedicated multicusp ion source, MIST-1 (generation-1 Multicusp Ion Source Technologies at MIT) [3], which is currently in the commissioning phase. The ion source will be producing a maximum of 20 – 50 mA of H_2^+ which must have a low emittance for efficient transport and injection into the cyclotron. Consequently, we would like to be able to measure the beam emittance. This is where the need for emittance scanners arises.

1.2 Beam Emittance

Beam emittance is a property of charged particle beams defined by the volume of a particle distribution in phase space, which is the coordinate system corresponding to the position and momentum coordinates of a particle (x, y, z, p_x, p_y, p_z) . Beam emittance is used along with physical dimensions such as radius to determine how the beam will evolve through the beam transport line. So it gives us valuable information to be used in design simulations.

Emittance is often observed through 'trace space.' Whereas phase space deals with position and momentum coordinates: x, y, p_x, p_y , trace space specifically looks at transverse motion through position and transverse angle coordinates: x, x', y, y' , with x' relating to p_x through:

$$p_x = m_0 c \beta \gamma x', \quad (1.1)$$

where m_0 is the rest mass of the particle and β, γ are the relativistic parameters. A similar relation holds for y' and p_y [4]. This is known as the paraxial approximation and is applicable when the transverse momentum components are small compared to the longitudinal which is true for our beam.

Emittance for a particular plane (such as $x - x'$ or $y - y'$), is the area of the ellipse created in trace space. This ellipse contains the entire particle distribution in that space, mathematically represented by the equation:

$$\varepsilon = \gamma x^2 + 2\alpha x x' + \beta x'^2, \quad (1.2)$$

with γ, α , and β being called Twiss parameters (not to be confused with the relativistic β, γ), related through the Courant-Snyder Invariant:

$$\gamma\beta - \alpha^2 = 1. \quad (1.3)$$

A typical ellipse in trace space is exemplified in Fig. 1-1.

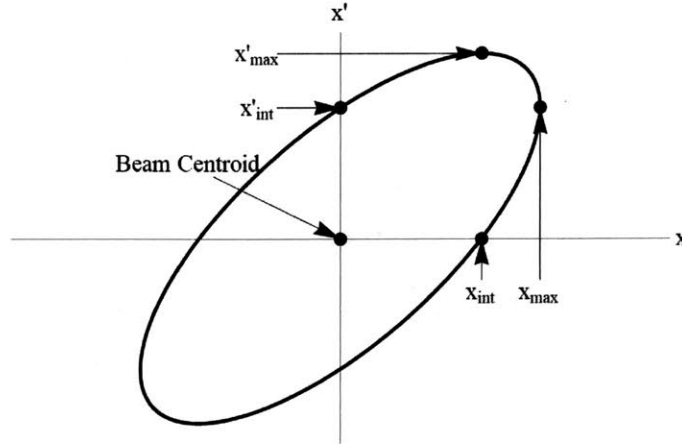


Figure 1-1: A plot of a typical trace space ellipse, specifically in the $x - x'$ plane, with points of interest labeled: $x'_{max} = \sqrt{\gamma\varepsilon}$, $x'_{int} = \sqrt{\frac{\varepsilon}{\beta}}$, $x_{max} = \sqrt{\beta\varepsilon}$, $x_{int} = \sqrt{\frac{\varepsilon}{\gamma}}$.

It is important to note the distinction between a model beam and a realistic beam. The previous theory has been for an idealized emittance, but for a realistic beam, the ellipse in trace space will vary in form. Thus for the actual measurement and analysis, we use what is called rms emittance [7]. It is expressed as

$$\varepsilon_{x,rms} = \sqrt{\langle x^2 \rangle \langle x'^2 \rangle - \langle xx' \rangle^2} \text{ [mm-rad]}, \quad (1.4)$$

for the $x - x'$ plane, with the second moments given by

$$\langle x^2 \rangle = \frac{\iiint x^2 f(x, y, x', y') dx dy dx' dy'}{\iiint f(x, y, x', y') dx dy dx' dy'}. \quad (1.5)$$

Both $\langle x'^2 \rangle$ and $\langle xx' \rangle$ are defined similarly, and the $y - y'$ emittance can be calculated in an identical manner.

1.3 Measuring Emittance

There are several types of emittance scanners, yet they all have the same general tasks to fulfill in order to obtain a suitable emittance measurement. As was mentioned earlier, emittance is measured in trace space (Fig. 1-1). For the spatial coordinate axis, a scanner will need some physical aspect to either encompass the entire length

of the coordinate (x or y) or some mechanism to sweep through it. For the transverse angle coordinate (x' or y') axis, a scanner will need a way to vary the angle of particles that it accepts for measurement, often through manipulation of geometry.

The following is a selection of well-established methods for measuring emittance:

- Wire emittance scanners [11], which as the name suggests makes use of wire to carry out the measurement. The wire (made of tungsten for example) determines the spatial coordinate with the orientation it intersects the beam, and its movement through the beam is actuated by a stepper motor. The signal is collected through the amount of charge hitting the wire, and through use of multiple wire scanners the beam emittance can be measured.
- Slit-grid scanners [10]. As per the name, these scanners involve both a slit and grid placed in way of the beam, the grid being made of a number of wires and parallel to the slit. These two are moved synchronously by a stepper motor which accounts for the sweep through spatial coordinates. As a ribbon of beam is passed through the slit, the angular distribution for that particular spatial coordinate is projected onto the grid and measured. In this case, there is no need to sweep through different transverse angle coordinates. Thus, the emittance can be measured with only worrying about the mechanical movement of the scanner during operation.
- Pepper-pot scanners [9]. The characteristic feature of this scanner is the pepper-pot plate, which is similar to the front slit plate from the slit scanner except that it has an array of holes rather than just a slit. Then, instead of a grid, the pepper-pot plate is combined with an ion detector (e.g. multi-channel plate, phosphor screen, and ccd camera combination). Thus, as the beam passes through the pepper-pot plate, the beamlets exiting the holes project onto the ion detector, and the image of those projections give information on the transverse angle coordinates. The spatial coordinates are determined by sweeping the pepper-pot plate through the beam. The pepper-pot scanner design also allows for a full 4D phase-space distribution measurement of a beam.

- Allison Emittance Scanners [2]. All the components for emittance measurement are housed into one compact box. The beam enters into the scanner head box through a thin slit at the front. Once inside, two deflector plates held at a voltage, as well as the geometry of the box, determine whether a particle will be measured by the collector assembly in the back. By varying the voltage on the deflector plates, different transverse angles of particles are allowed to be collected and measured. As for the spatial coordinates, the entire scanner is simply driven by a stepper motor through the beam to get the full x or y axis.

We ultimately went with the Allison scanner design due to its compactness, simplicity, and high resolution. It is a well-established design with readily available documentation of its implementation. One drawback is that it only allows measurement of the uncoupled $x - x'$ and $y - y'$ planes, whereas the pepper-pot scanner for example can give a fuller picture of a beam's emittance with interactions across the x , x' , y , and y' coordinates. However, slit-grid and pepper-pot scanners are more limited in resolution than Allison scanners, which we feel makes up for the missing correlation data.

Chapter 2

Emittance Scanner Hardware

The emittance scanners are something that we built from the ground up. We began with designing them on the CAD software Autodesk Inventor through inspiration from known models, then had them built in MIT's Central Machine Shop, and finally assembled and installed them into vacuum in line with our ion source beam line.

2.1 Design Considerations

The Allison Emittance Scanner is based on the work of Allison, Sherman, and Holtkamp [2], and a cartoon of its operation is depicted in Fig. 2-1. Its method of beam measurement begins with a thin slit at the front of the scanner which lets only a thin ribbon of beam into the scanner head. Inside are two charged deflector plates. Particles enter the scanner head at various initial angles, and due to the deflector plates, the particles will follow a curved trajectory as they travel through the head. Thus, depending on the voltage, only particles of a particular initial angle will follow the correct trajectory so as to pass through the exit slit and into the collector plate. All other particles will end up impinging on an interior surface.

By varying the voltage on the deflector plates, we are able to collect signal for different transverse angles (x' or y'). The following general steps are taken to build up a full emittance measurement:

- Begin at a spatial coordinate on the x or y axis.

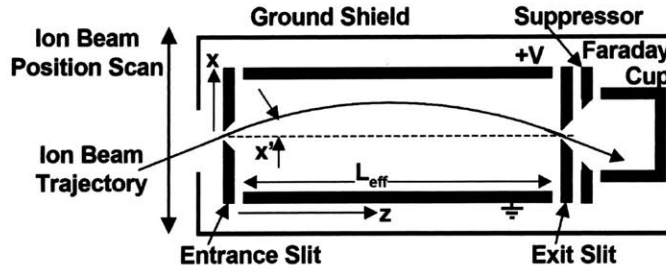


Figure 2-1: A graphic of how beam measurement takes place [12]. The beam enters through the entrance slit, and only particles of a certain initial angle will have the correct trajectory between the deflector plates to allow them to be collected for measurement.

- Vary the voltage, thereby collecting data for different transverse angles.
- Move the scanner to the next spatial coordinate and repeat the process.

Through this we are able to calculate the complete transverse x or y emittance for a particular longitudinal position.

2.1.1 Design Parameters

No matter the exact design of the scanner, there are several parameters that have to be considered and whose precision are crucial to allowing the physics to work out as desired. These parameters are the distances between certain components inside the scanner head, and the features they determine are:

- Amount of beam that enters the scanner head, thereby affecting resolution.
- The maximum initial angle of particles entering the scanner head, thereby affecting range.
- The maximum deflector voltage, again affecting range.

First we have D , the travel distance for the beam once it has entered the head. This distance is determined by two pairs of steel plates at the front and back of the head. Then there is the distance S between each pair of steel plates which determines the size of the slit through which the beam enters the head. Next there is the distance

g between the two deflector plates, and finally the distance δ between the deflector plates and the steel plates at each end. These parameters, along with the values we determined for them, are summarized in Table 2.1. They are also visualized in Fig. 2-2.

Table 2.1: Parameters that determine range, resolution, and size of the scanner. D is the length that the beam travels. S is the size of the slit between two steel plates through which the beam enters and exits the scanner box. g is the size of the gap between the two deflector plates and δ is the distance between the deflector plates and the steel plates at each end. These are design values and are not the actual measured distances. These dimensions are visualized in Fig. 2-2

Variable	Value
D	100 mm
S	0.05 mm
g	5.3 mm
δ	2 mm

From these parameters we are able to calculate various features and constraints for our measurements.

According to [2], the phase-space area resolution is given by:

$$\frac{S^2}{D}, \quad (2.1)$$

resulting in a (ideal) resolution of about 2.5×10^{-8} mm. This is further limited by the minimum step size of the linear actuator ($\sim 2.5 \times 10^{-5}$ mm). The maximum initial angle, X'_m , is given by:

$$X'_m = \frac{2g}{D + 2\delta}. \quad (2.2)$$

So given our chosen dimensions, our scan should be able to measure angles up to ± 100 mrad ($\sim 5.73^\circ$). The maximum deflector voltage is:

$$V_m = \pm \frac{8g^2\phi}{D^2 - 4\delta^2} \quad (2.3)$$

where ϕ is the ion potential. We chose a power supply capable of ± 1.5 kV leading to a maximum analyzable beam energy of ~ 66.7 keV.

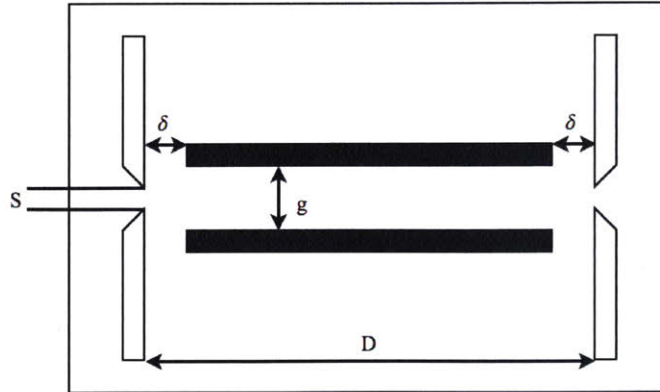


Figure 2-2: A visualization of the dimensions of the various components inside the scanner head. Seen here are the two deflector plates as the black bars in the middle, and two pairs of steel plates at each end as the tapered blank bars. These features can be seen in a rendering of the actual design in Fig. 2-3

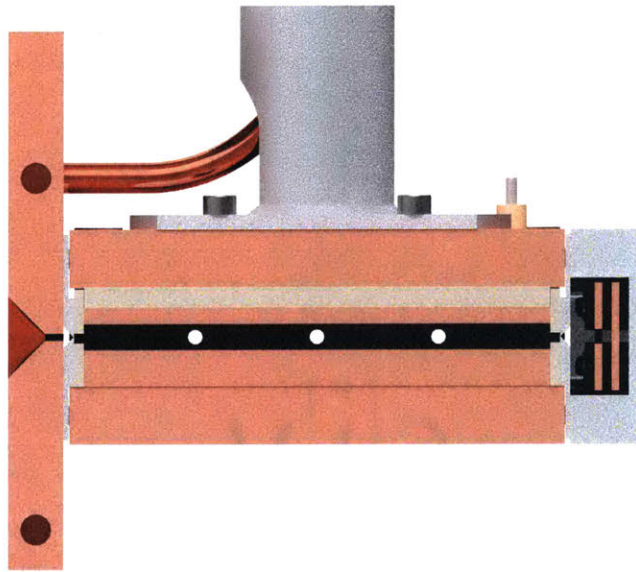


Figure 2-3: A rendering of a cut view of the scanner head displaying the inner components. In order to enforce the afore-mentioned dimensions from Table 2.1, front and back insulators between the steel plates and deflector plates determine the distance δ . g is determined by side t-insulators which separate the bottom and top deflector plates. The combined distance of deflector plate, front and back insulators were assured to be D , and slit width S was adjusted using a shim of thickness ~ 0.05 mm.

2.1.2 Heat Transfer

With 20 – 50 mA beam of current hitting the front plate of the scanner, heat transfer was an issue that had to be addressed. We incorporated a water cooling system into the front plate of the scanner, which is where most of the heat will be dissipated. We ran thermal simulations using the "Thermal Simulation" suite within Autodesk's Fusion 360, both for a 6 cm beam diameter and for a 1 cm beam diameter. As a worst case, we assumed a maximum beam current of 50 mA and maximum energy of 80 keV. This translates to a beam power of 4 kW.

In order to run the simulations on the water cooling system there are various parameters that had to be assumed and estimated. First, the material of our front plate is polished copper. We assumed that the water would be entering the front plate at 20° C and increase by a maximum of 20° C, thus exiting at around 40° C. In addition, we assumed the total length that the water travels both through the front plate and external tubing to be 4.2 m. This takes into account the planned positioning of the scanner relative to our water supply manifold. We also know that the inner diameter of the water lines is 0.2 in.

From this and a pressure gradient of 30 psi, we calculated that the water cooling system would be able to draw heat away from the front plate at about 4.5 kW, which is satisfactory. After running the simulations, we observed that for the 6 cm beam diameter, the front plate would reach a maximum steady-state temperature of about 70° C. For the 1 cm beam diameter, the front plate was shown to reach a maximum temperature of about 480° C. These values indicate minimal potential for damaging the scanner.

2.2 Detailed Design

The entire detailed design of our emittance scanner system includes the scanner, stepper motor, electrical and water connections, and vacuum equipment. A rendering of this can be seen in Fig. 2-4.

The scanner itself (excluding vacuum pipes and stepper motor) can be separated

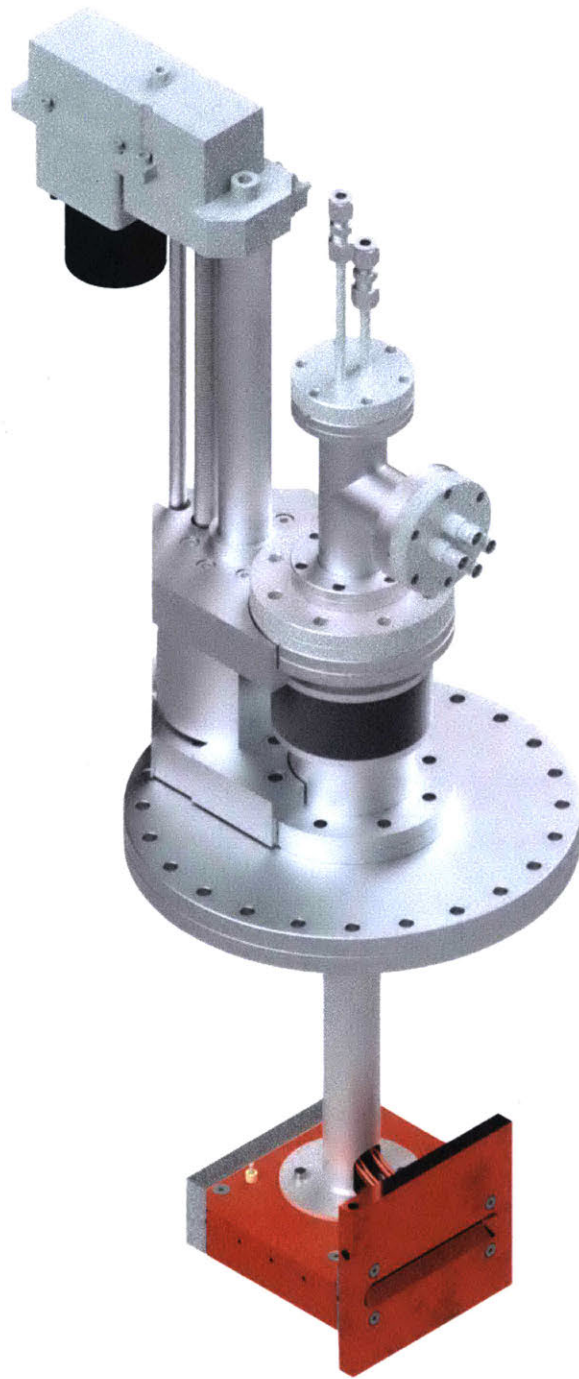


Figure 2-4: A rendering of the full emittance scanner system including the scanner, stepper motor, vacuum equipment, and electrical and water connectors.

into three main parts: the front plate, the scanner head, and the collector assembly.

The front plate is the simplest. It has water cooling channels, a slit through which the beam first enters, and two copper water pipes brazed onto the back of it. In an initial iteration of design, the front plate was flush with the rest of the scanner box, but in the final design we decided to extend it vertically both ways as a precaution to prevent the beam from damaging the rest of the structure (e.g. cables) as the scanner moves through it.

The scanner head consists of a lower and upper copper shell. These two screw together, creating an enclosure for the rest of the inner components. The contents include the two deflector plates, two pairs of stainless steel plates at the front and rear, and various insulator parts. For all these parts we adopted a compression method to keep them together correctly: pieces fit together by resting on each other and being precisely the right length to allow compression to secure them into place. For this, keeping tolerances in mind was extremely important. Thus by screwing the front plate, scanner head, and rear assembly all together, the contents of the scanner head are completely held in place. In addition, a pin is fit into the upper deflector plate and cleared to stick out of the top of the scanner head. This is how the voltage is applied to it. An exploded view of the scanner head can be found in Fig. 2-5.

The rear assembly largely consists of an aluminum housing piece. Within it is placed both an electron suppressor plate and collector plate, separated by insulator pieces. These two are in contact with different screws from the outside of the aluminum housing piece. This is how the electron suppressor plate is applied a voltage and how the collector plate's signal is measured. An exploded view of the rear assembly can be seen in Fig. 2-6

Attached to the top of the scanner head is a stainless steel pipe, the design of which posed some challenges. Given the rigidity of the copper water pipes and the need to both connect them to water supply and subsequently keep them housed within the vacuum equipment, we went with a telescopic design for the stainless steel pipe. This telescopic design allows us to slide the copper water pipes up until they stick out from the flange, connect them to the water feedthroughs, then slide it back down

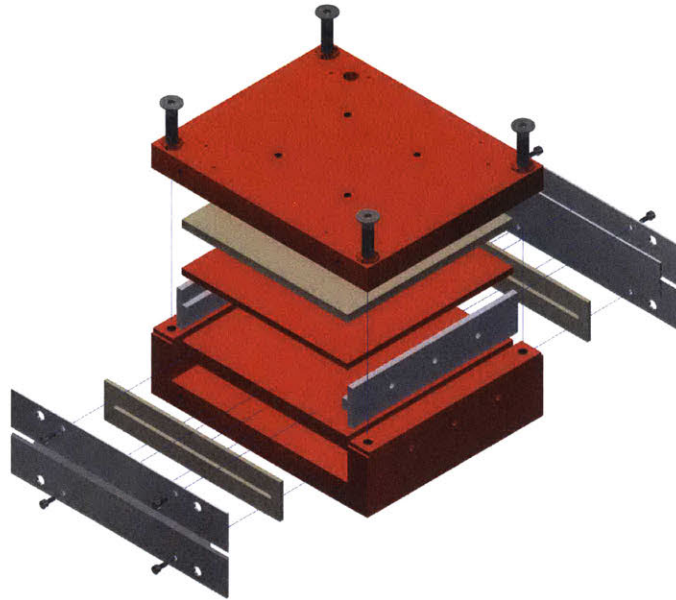


Figure 2-5: An exploded view of the scanner head, displaying all the inner parts. The lower deflector plate rests at the bottom of the lower copper shell. Two t-insulators rest on both sides of the deflector plate. This creates a gap between the next deflector plate that gets stacked on. Then there is an insulator piece on top, right before the upper copper shell. Furthermore, there are two more insulator pieces with slits on the front and back placed inbetween deflector plate and stainless steel plate. The only pieces that contain screws are the copper shells and stainless steel plates.

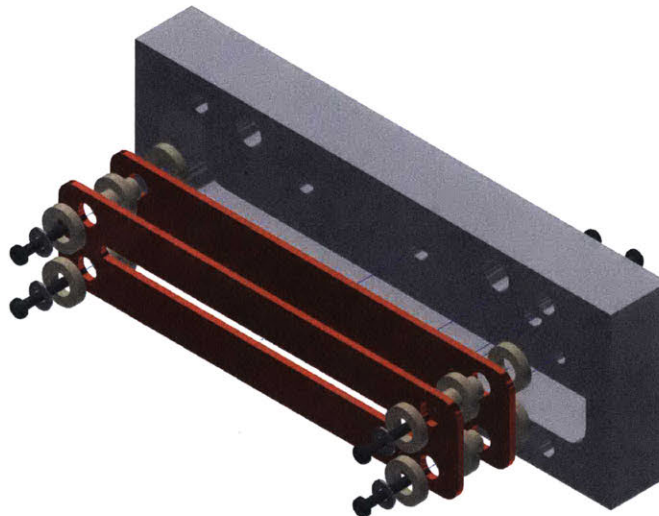


Figure 2-6: An exploded view of the rear collector assembly. The copper plate closer to the viewer and with the slit in the middle is the electron suppressor plate. The copper plate closer to the aluminum housing is the collector plate.

and screw the two telescopic pipe pieces together. We also included use of a vacuum t-piece in order to split the water feedthroughs from the electrical feedthroughs. And so both the copper water cooling pipes and electrical cables travel through this pipe to be connected to their respective sources outside of the assembly. This pipe and vacuum t-piece structure is itself attached to the stepper motor.

Drawings for all the CAD model assemblies can be found in Appendix A. Two such scanners were machined and constructed, one to be installed horizontally on our six-way cross to measure the $x - x'$ emittance, and one to be installed vertically to measure the $y - y'$ emittance.

Chapter 3

Controls and Data Acquisition

In this chapter I will describe the hardware and software used to control the scanners and record data.

3.1 Hardware

The hardware involved in this project is centered around powering and operating the scanners. Starting with the contents of the scanners, an important aspect is receiving the signal from the collector plate. This is accomplished with a Keithly 6485 Picoammeter. It connects to the collector plate through a BNC cable. The picoammeter in turn is connected to a computer where the signal current can be read and recorded. Next, a voltage of -200 V has to be applied to the suppressor plates. This is done using a voltage power supply connected through a BNC cable. Then there are the deflector plates which are powered by a ± 1.5 kV Matsusada AP-1.5B(A) HV amplifier and connected through an MHV cable. In order to sweep the voltage, an intermediate device had to be used between the computer and the high voltage power supply for communication. For this we used a National Instruments (NI) voltage output device which allows us to both vary the voltage on the high voltage power supply and read it back on the computer

We are using a McAllister Technical Services linear actuator with bellows, driven by a stepper motor. This is powered by its own control box and it communicates with

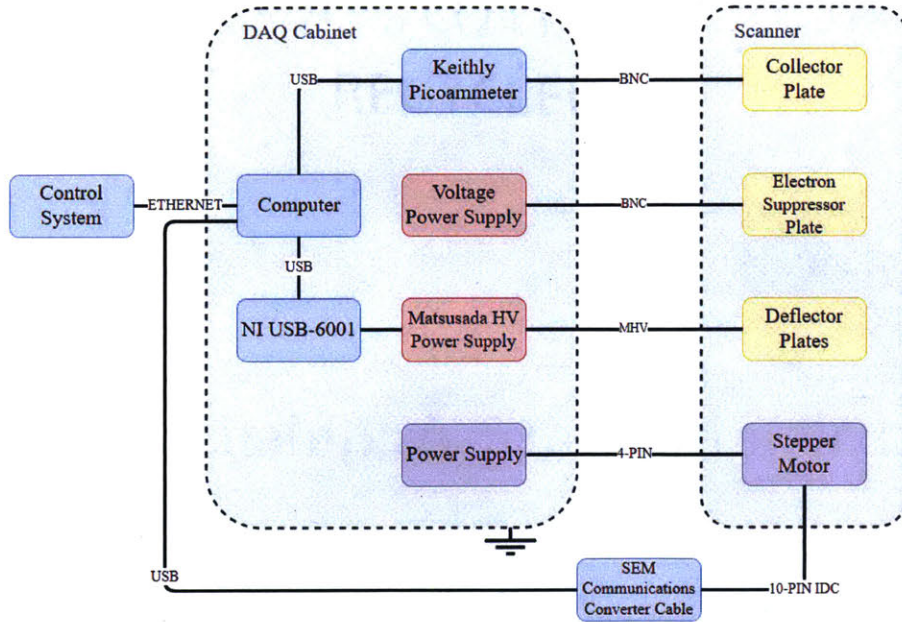


Figure 3-1: A diagram of the hardware involved with this project. They are mostly separated into two main sections: those housed inside our data acquisition cabinet, which is grounded, and those involved more directly with the scanners. In addition, the blocks in blue are electrical-data acquisition devices, those in red are power supplies, those in violet are electro-mechanical devices, and those in yellow are electrostatic electrodes.

the computer through an SEM Communications Converter Cable. The computer handling all these devices is connected through ethernet to our main control system computer. A diagram of the hardware can be seen in Fig. 3-1.

3.2 Software

The software for this project involved writing programs for each of the devices so as to operate all of them remotely from our control system. This includes software drivers for the stepper motor, the high voltage, and picoammeter.

For the stepper motor, we need to be able to send the appropriate commands to move the scanners to desired locations. Particularly for conducting the scan, we need to move by discreet distances for each step after a measurement. Establishing a "parked" position is also important given that we have two scanners installed: one vertically and one horizontally. Thus it is necessary to have one scanner be completely

out of the way before the other one can be operated. Also, we need software checks to prevent movement of one scanner while the other one is being operated.

The high voltage amplifier is controlled through an NI-6001 Digital Analog Converter (DAC), capable of outputting a signal in the range of -10 V to $+10$ V. By implementing the NI software libraries, we are able to convert the voltage signal from the DAC to the high voltage amplifier, thus letting us charge the deflector plates. Some noise is built up due to this additional component in voltage supply, so a 500 sample average is applied.

The picoammeter takes in the signal collected from the collector plate, which is read out and displayed on our control system computer. This is our main device for data acquisition

All these software drivers are controlled through a user interface that takes input values to set the various parameters. For example, to conduct a scan, a minimum, maximum, and step value is input for both the stepper motor and the voltage. Thus, for a give position, the control system computer will have the high voltage power supply step through the voltage range, readout the charge from the picoammeter for each voltage, then move on to the next position step and do the same.

Chapter 4

Preliminary Commissioning

4.1 Experimental Setup

For testing and commissioning, the two emittance scanners were installed in a new six-way cross and attached to the existing ion source setup. The layout can be seen in the photograph in Fig. 4-1. The source is attached to a six-way cross under high vacuum and supported on an aluminum structure. The source itself is kept within a high voltage cage, while the rest of the vacuum equipment is outside on a ground potential. Attached to this six-way cross is also a faraday cup (for measuring the beam current), and ion gauges to measure the pressure. Opposite to the ion source is a second six-way cross attached to the first. This is where the scanners were installed: one on top and one at the side. So the beam travels the distance of the first six-way cross before reaching the scanners.

The emittance scanner systems are connected to a water supply for cooling with a supply and return connection at the top of the stepper motor. They are connected to the data acquisition cabinet through a three-pin electrical feedthrough: one each for signal, electron suppressor, and high voltage.

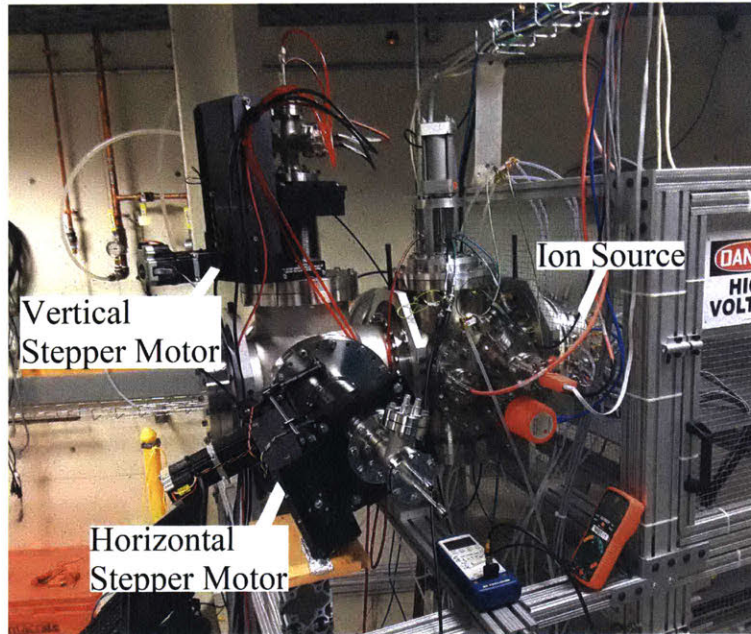


Figure 4-1: A photo of the laboratory setup. On the right, inside the high voltage cage, is the ion source. It is attached to a six-way cross, which at the opposite end to the source is attached to another six-way cross. It is on this one that the two emittance scanner systems are installed, one vertically and one horizontally.

4.2 Commissioning Results

Time did not permit a full commissioning of the system. We were able to conduct a test measurement before which we had to take the following tasks:

- Test the high voltage.
- Make sure all the devices were working properly, such as DAC device, picoammeter, etc.
- Check that all the peripherals for the devices were responsive on the computer.
- Test the stepper motor calibration.
- Ensure the scanner would pass through the entire beam, done by adjusting limit switches which designate physical positions where the stepper motor stops moving.

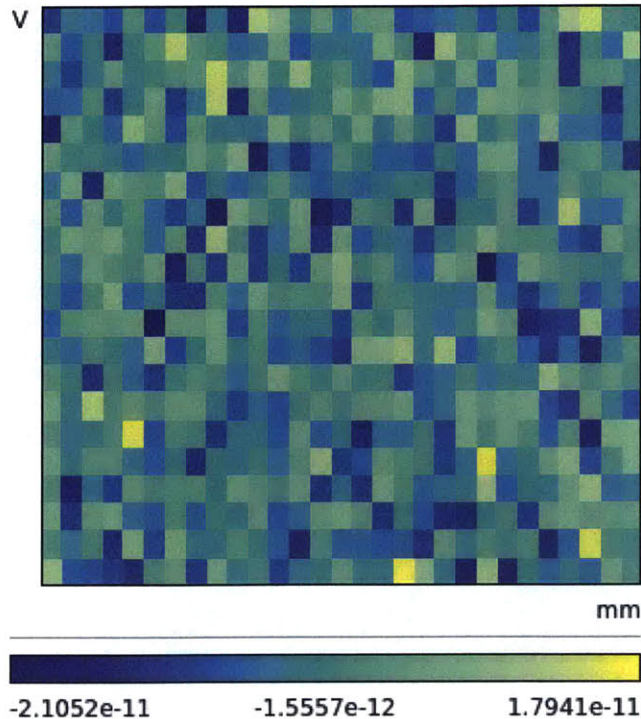


Figure 4-2: Raw scan data with no beam, showing the noise of the picoammeter.

We first performed a scan with no beam to get information on the noise present from the picoammeter. A plot of this is found in Fig. 4-2. The mean of this noise is -1.55×10^{-12} A with a standard deviation of 6.75×10^{-12} A.

Time did not permit for a complete measurement, but we were able to perform preliminary commissioning with a $15 \mu\text{A}$ beam. A plot of this scan can be seen in Fig. 4-3. Analysis performed on this scan can also be seen in Fig. 4-4.

The emittance scan produces a 2D histogram with current as the binned data for each coordinate pair of (x, V) . Using an existing analysis program written in python, the voltage is first converted to transverse angles x' using the geometry of the scanner (Eq. 2.2 and Eq. 2.3). Furthermore, the program makes use of Eq. 1.4 and Eq. 1.5.

Table 4.1: A table of the two normalized emittances we calculated from the collected data, one for 1 RMS and one for 4 RMS

Normalized Emittance	Value
1 RMS	0.036 π -mm-mrad
4 RMS	0.144 π -mm-mrad

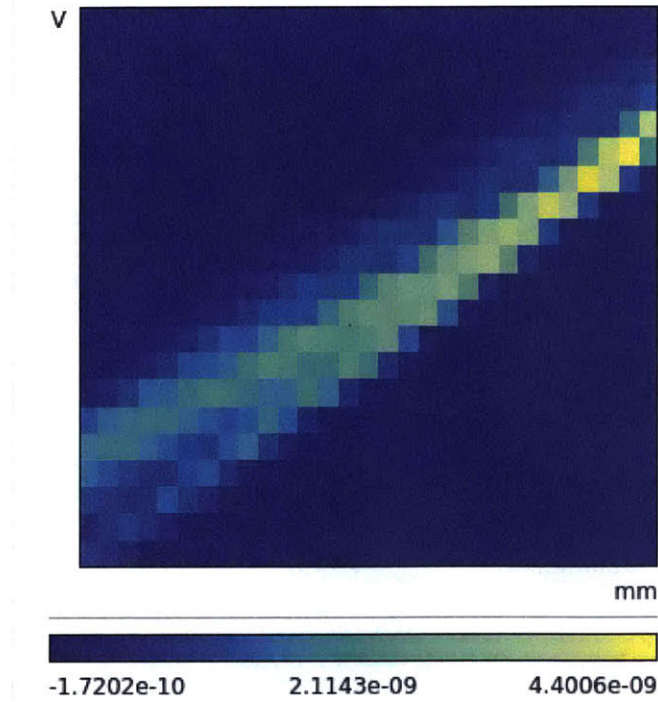


Figure 4-3: Raw scan data with a $15 \mu\text{A } H_2^+$ beam entering the scanner.

The distribution of current on the emittance histograms can be taken as the function in the moment equation, thus the second moments of x , x' , and xx' can be calculated, thereby giving the rms emittance for x with the rms emittance equation.

From this we calculated the normalized emittances which can be found in Table 4.1. The Twiss parameter for this emittance are: $\alpha = -2.46$, $\beta = 0.16 \text{ mm/mrad}$, and $\gamma = 40.21 \text{ mrad/mm}$.

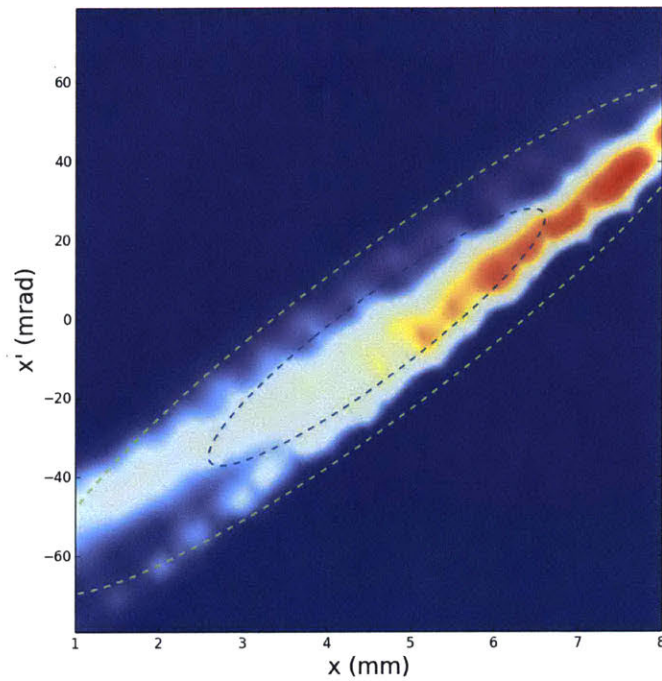


Figure 4-4: An analysis using an existing program written in python on the first emittance scan (Fig. 4-3) for a $15 \mu\text{A}$ beam. The inner ellipse is 1 RMS which includes 58.3 % of the beam, and the outer ellipse is 4 RMS which includes 97.3 % of the beam. Note that the beam is clipped left and right, which will statistically reduce the emittance value. Time did not permit retaking the scan with wider limits.

Chapter 5

Conclusion

5.1 Summary

I developed an emittance scanner to be used in the low-energy beam transport part of the IsoDAR experiment. This development involved consideration of various scanner designs before settling on the so-called Allison Emittance Scanner due to its simplicity and high resolution. This was followed by designing the scanner through CAD software and detailing it before having the parts machined. Additional work went into the water cooling system, powering of the devices, and data acquisition method.

We had two emittance scanners assembled and installed into vacuum along with our ion source where preliminary commissioning scans were performed, one used for vertical emittance measurement and the other for horizontal. We were able to collect data for the noise present in the system along with results for the $x - x'$ emittance of a $15 \mu\text{A}$ beam.

5.2 Outlook

We achieved preliminary commissioning with the emittance scanners, yet there are still several steps to take to establish a full commissioning, which I will continue working toward in the coming few weeks. These steps are:

- Systematic tests of the control and DAQ electronics (power supplies, high volt-

age amplifier and picoammeter) to obtain calibration curves and realistic error estimates.

- Alignment of the emittance scanner heads with respect to the beam center by adjusting the limit switches, and careful calibration of the stepper motor movement.
- A full error propagation study for the calculated emittance. This will take into account systematic and statistical uncertainties obtained from the calibration process, data sheets, and during the measurement itself.
- Several test measurements with beam from the MIST-1 ion source using both the vertical and horizontal emittance scanners.

Appendix A

Assembly Design Drawings

42

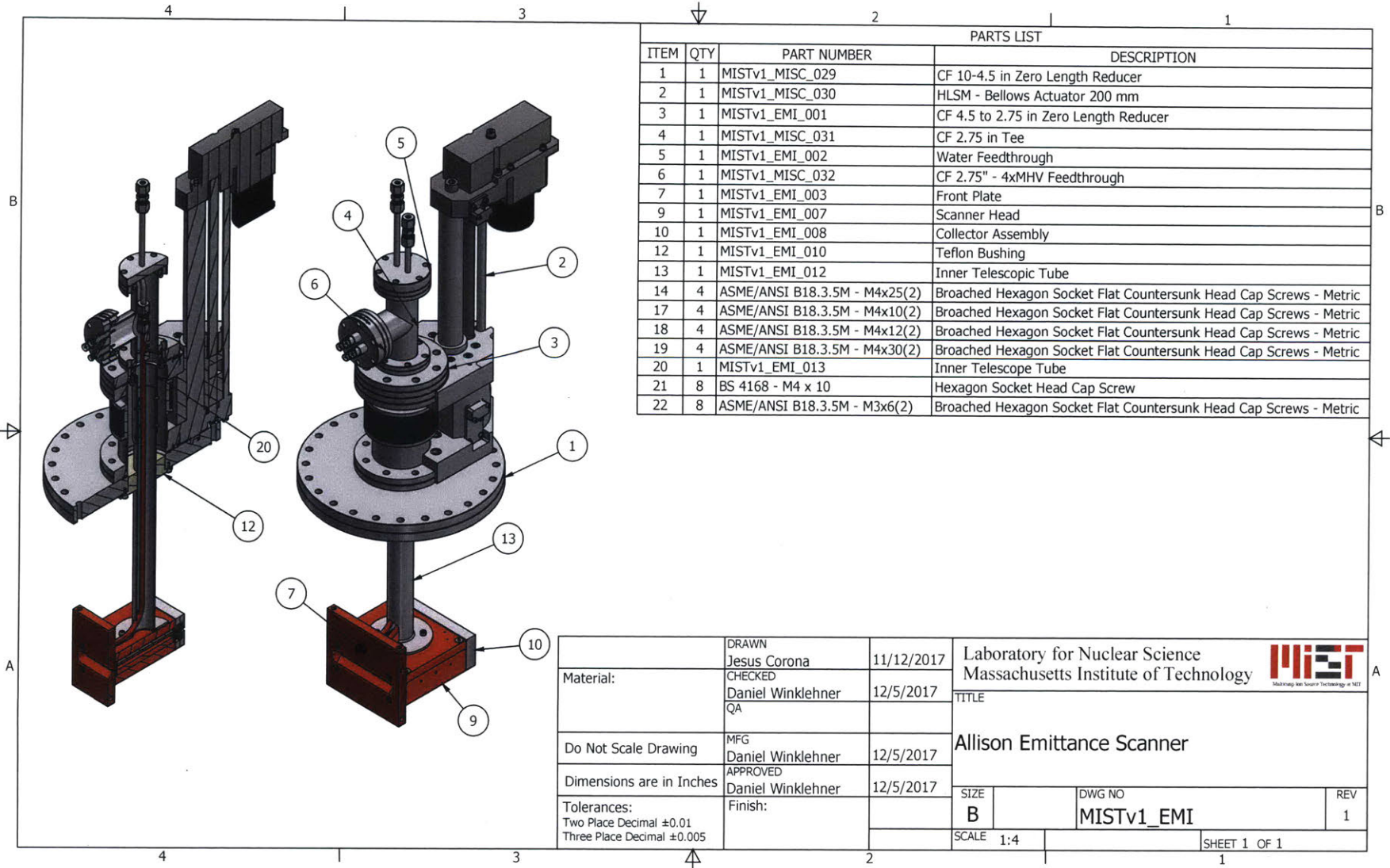


Figure A-1

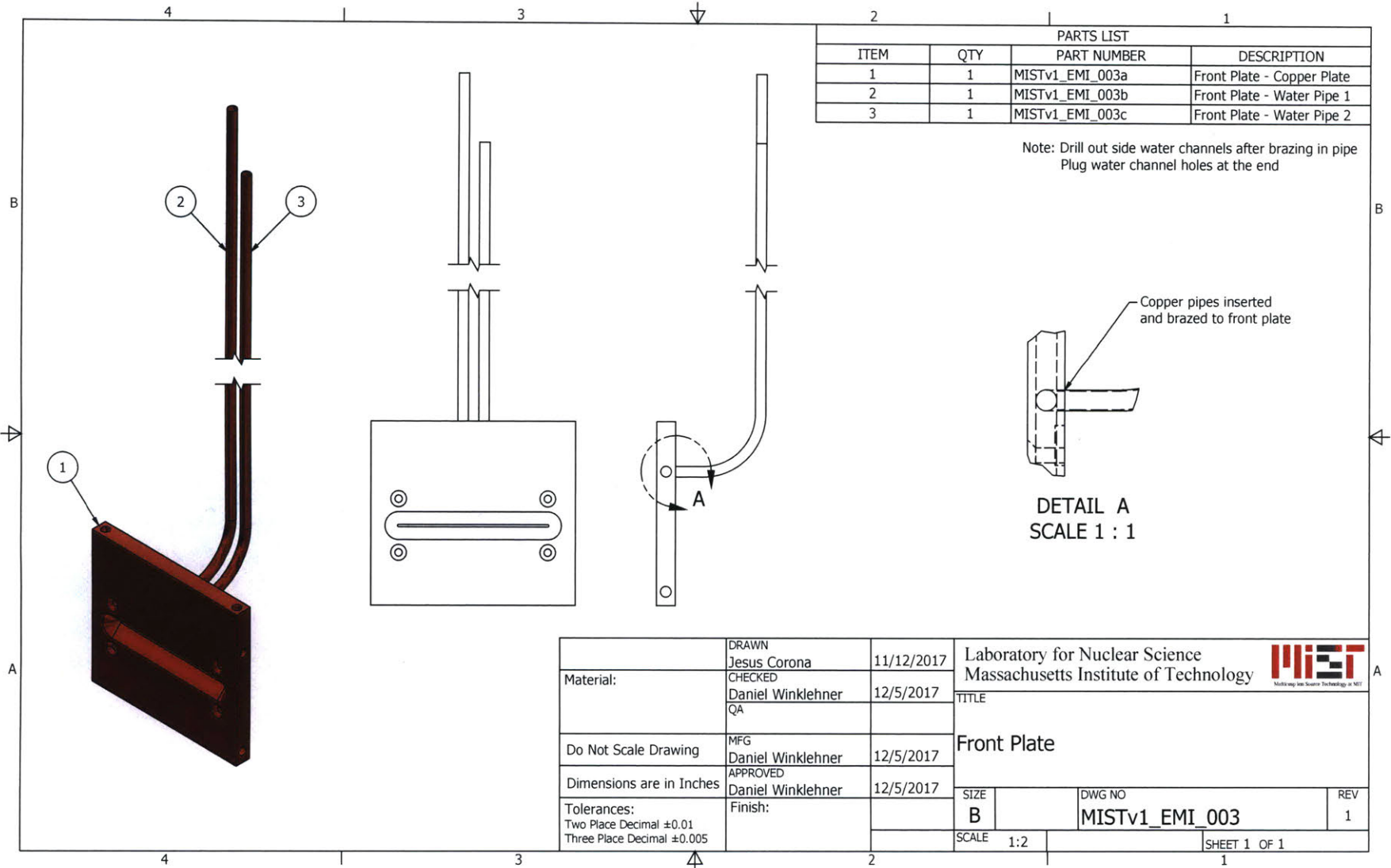


Figure A-2

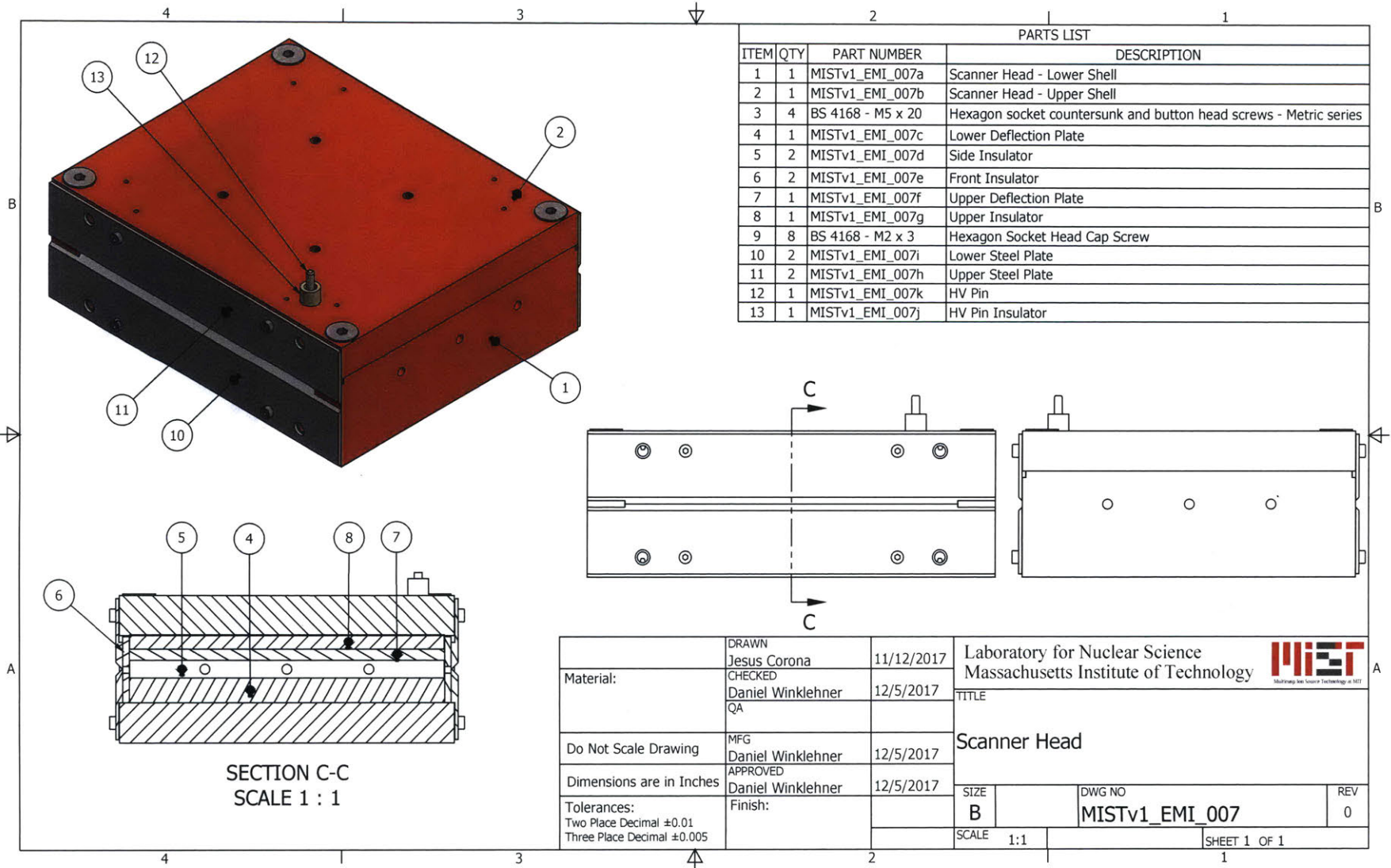
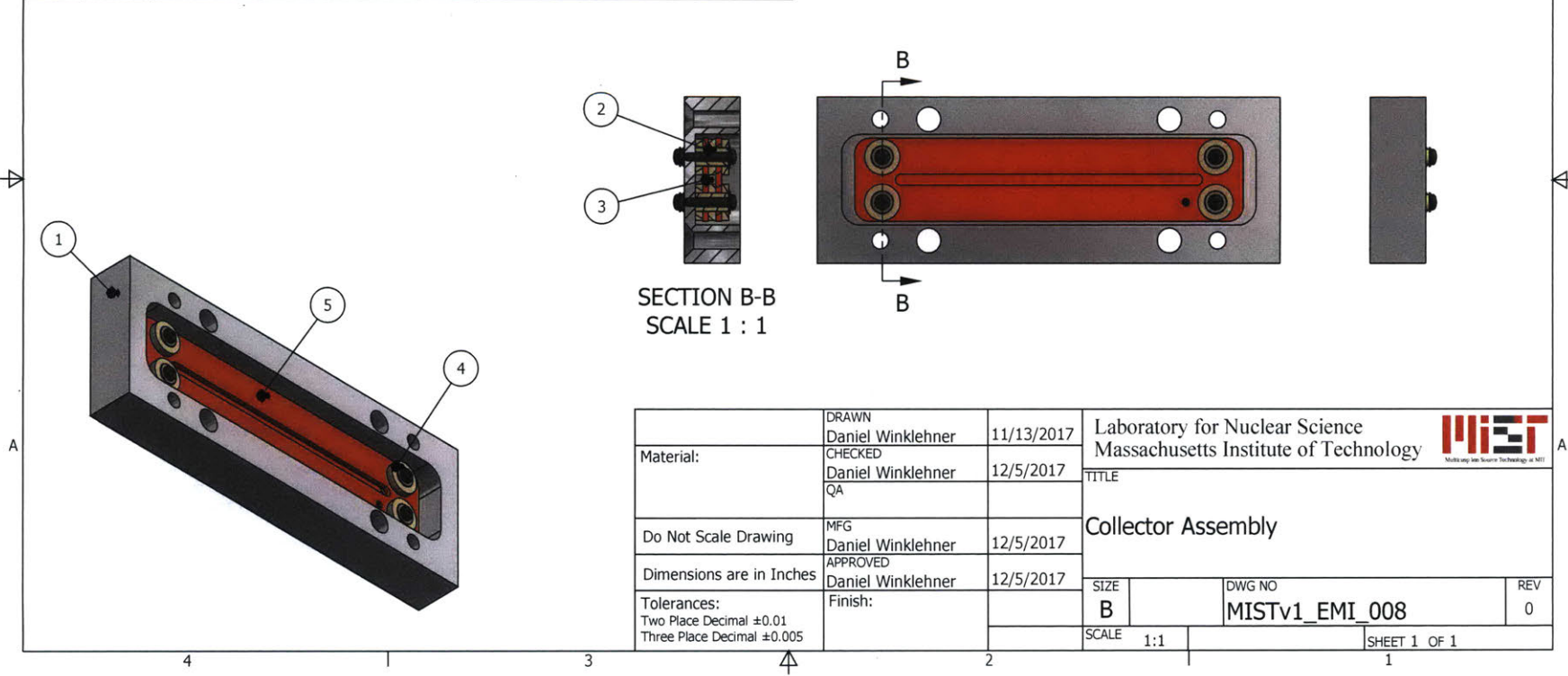


Figure A-3

PARTS LIST			
ITEM	QTY	PART NUMBER	DESCRIPTION
1	1	MISTv1_EMI_008a	Collector Housing
2	4	MISTv1_EMI_008c	Insulator Tube
3	1	MISTv1_EMI_008b	Collector Plate
4	12	MISTv1_EMI_008d	Insulator Ring
5	1	MISTv1_EMI_008e	e-Suppressor Plate
6	4	DIN 125-2 - A 2.5	Washer
7	5	ISO 7045 - M2 x 12 - 4.8 - H	Cross Recessed Pan Head Machine Screw
8	2	MISTv1_EXT_005	SCM 2X3 Screw Insulator
9	4	DIN 125-2 - A 2.2	Washer
10	1	ISO 7045 - M2 x 8 - 4.8 - H	Cross Recessed Pan Head Machine Screw
11	2	ISO 7045 - M2 x 3 - 4.8 - H	Cross Recessed Pan Head Machine Screw



Material:	DRAWN Daniel Winklehner	11/13/2017	Laboratory for Nuclear Science Massachusetts Institute of Technology	
	CHECKED Daniel Winklehner	12/5/2017		
Do Not Scale Drawing	MFG Daniel Winklehner	12/5/2017	TITLE Collector Assembly	
	APPROVED Daniel Winklehner	12/5/2017		
Tolerances: Two Place Decimal ±0.01 Three Place Decimal ±0.005	Finish:	SIZE B	DWG NO MISTv1_EMI_008	REV 0
		SCALE 1:1	SHEET 1 OF 1	

Figure A-4

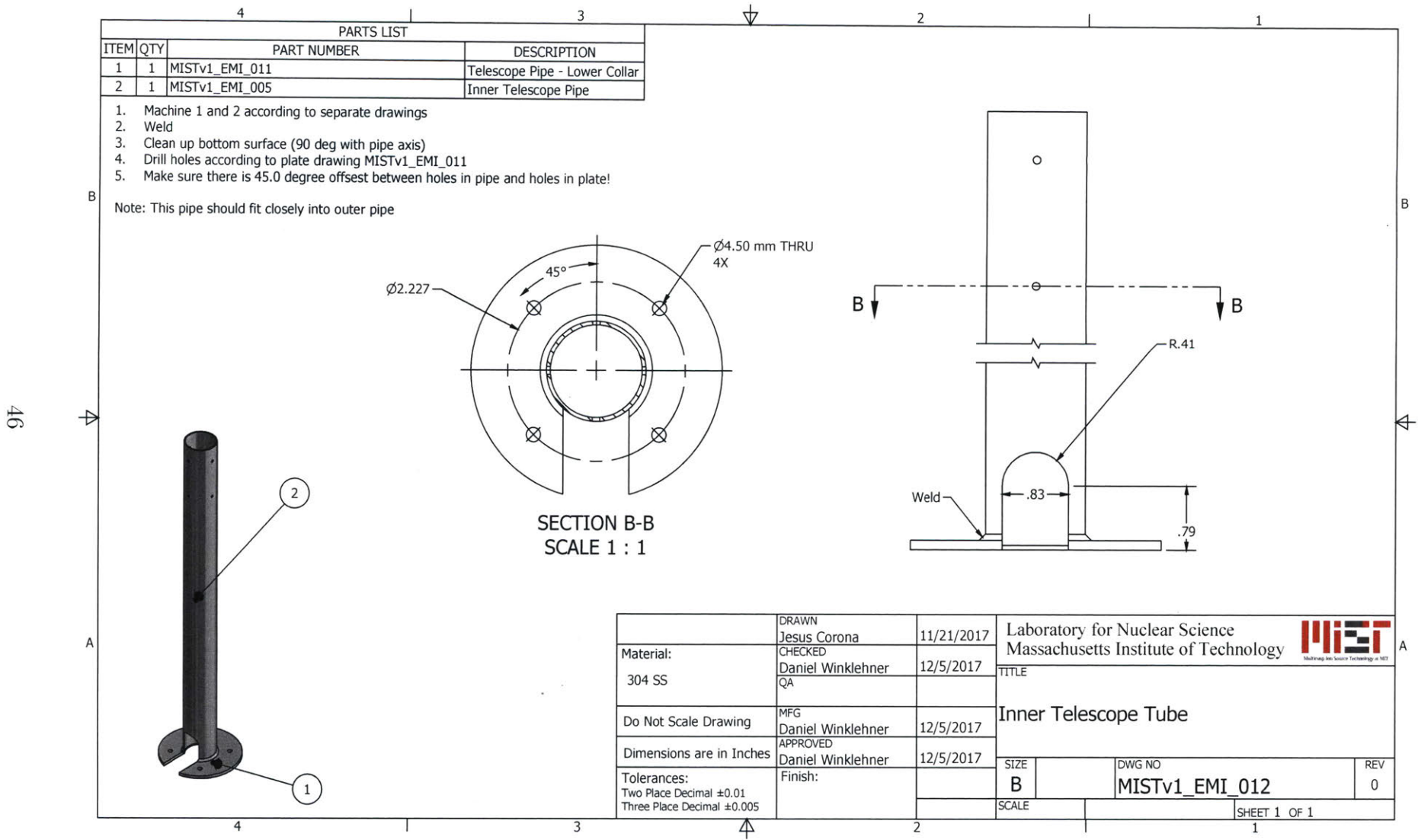


Figure A-5

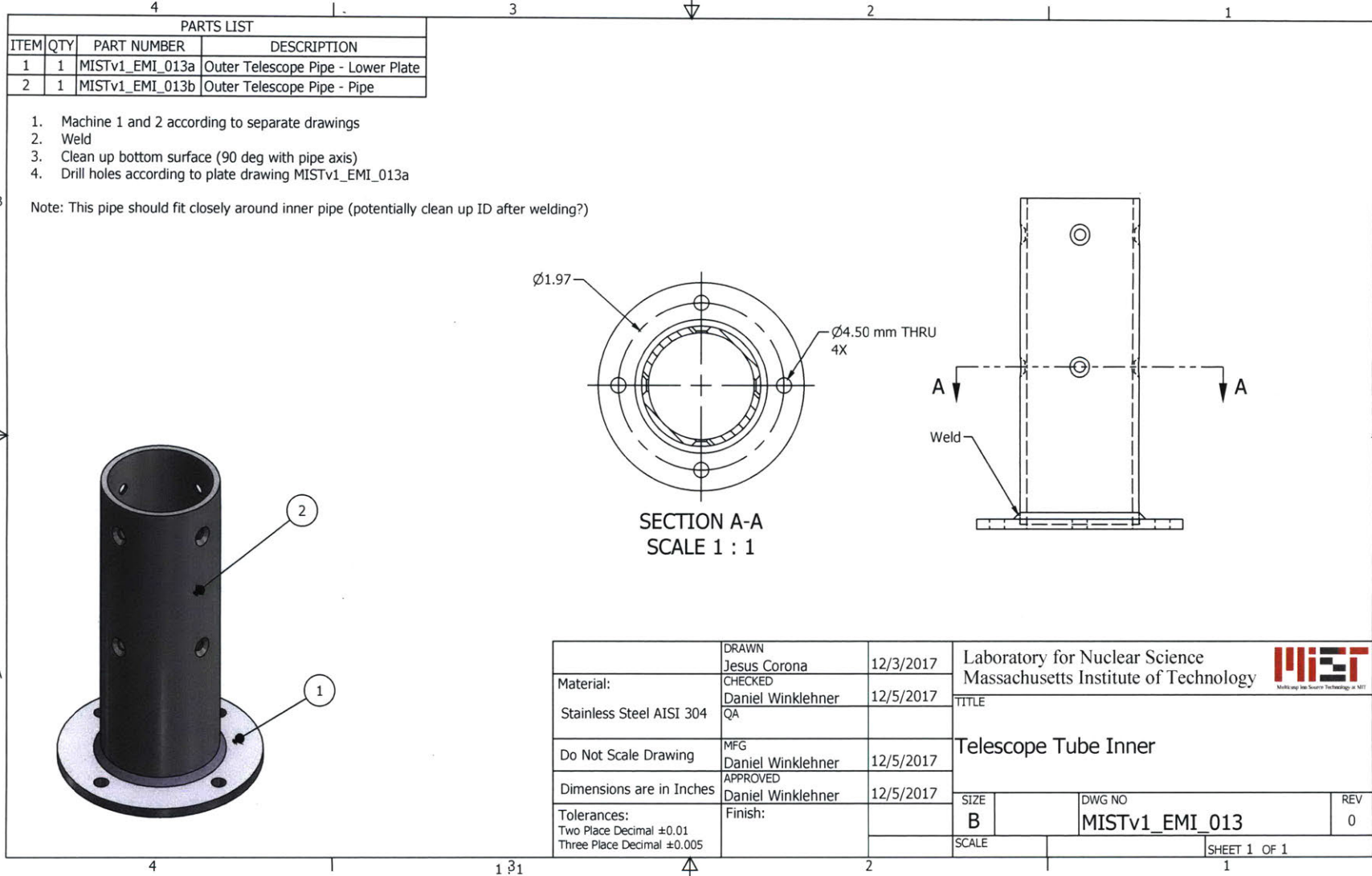


Figure A-6

Appendix B

Installation Photos

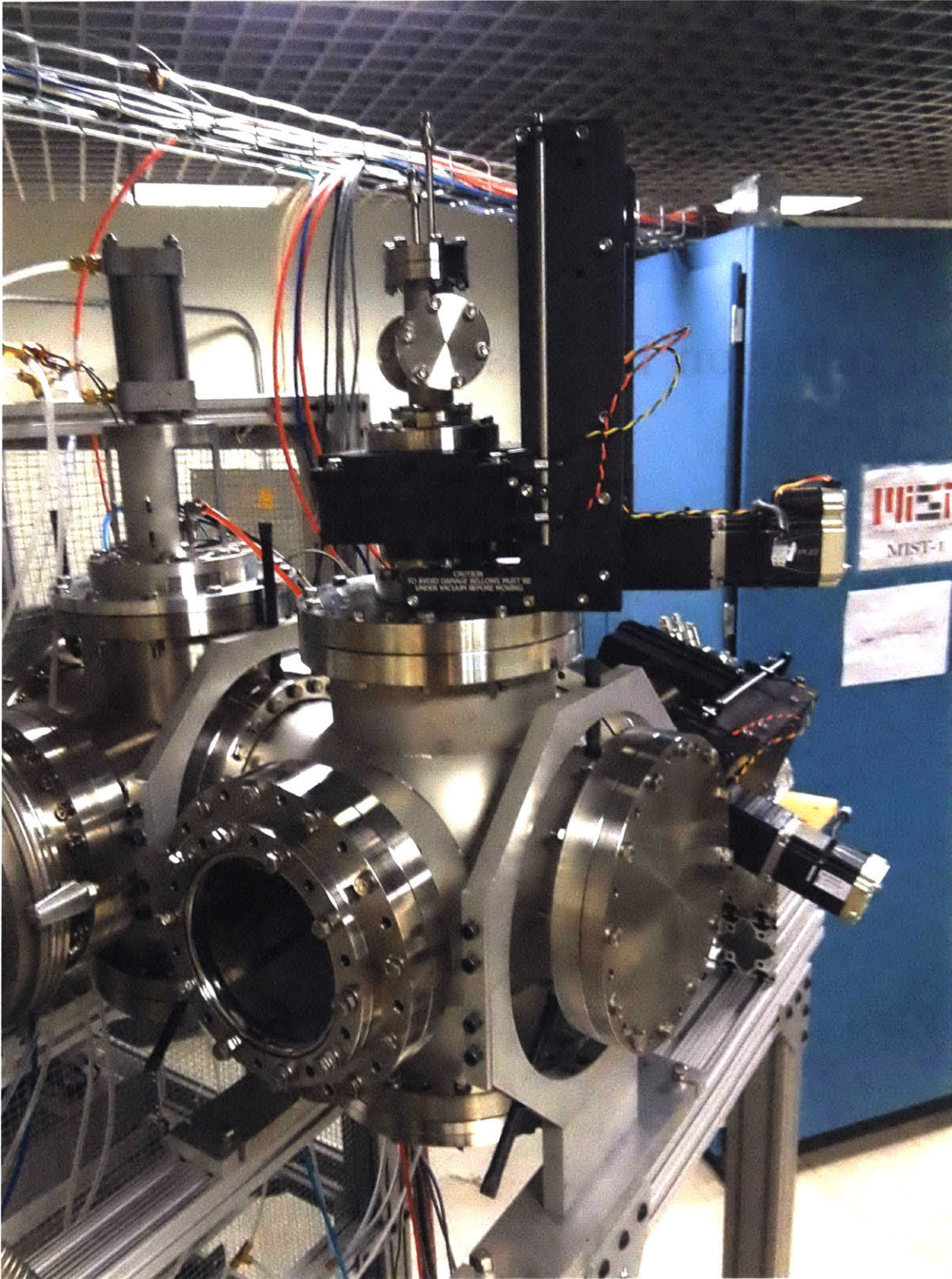


Figure B-1: Seen here is the six-way cross with vertical emittance scanner-stepper motor system installed. The stepper motor (in black) is fully retracted, meaning the scanner is lowered within the six-way cross. On top of the stepper motor is the vacuum t-piece which has water feedthroughs on the top flange and electrical feedthroughs on a side flange (not in view)

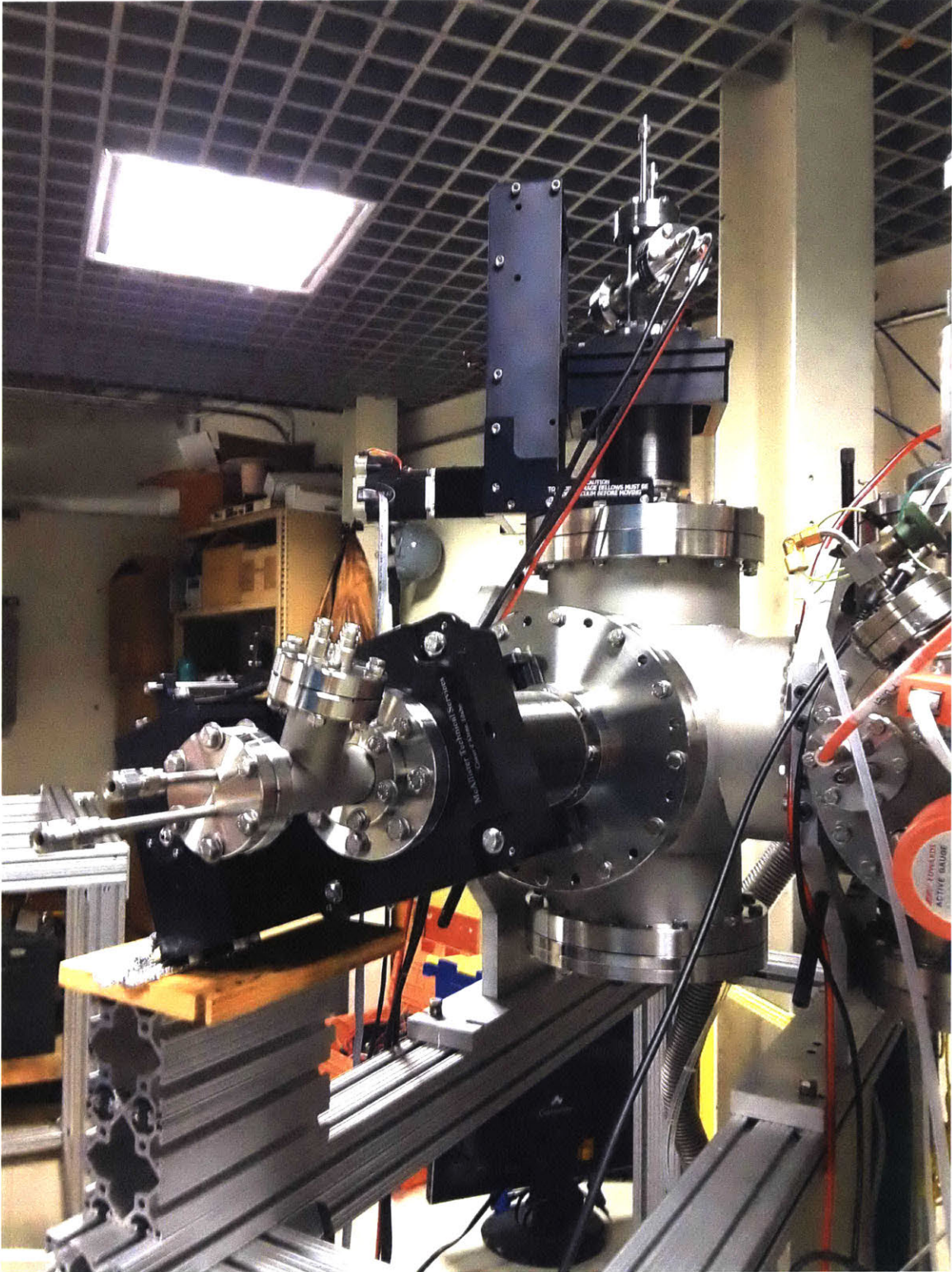


Figure B-2: A view of the installation of the horizontal emittance scanner-stepper motor system. This one is extended as noted by the exposed bellows visible near the flange, so the horizontal scanner is parked within the side of the six-way cross while the vertical scanner is positioned in the center.

Bibliography

- [1] S. Abe, T. Ebihara, S. Enomoto, K. Furuno, Y. Gando, K. Ichimura, H. Ikeda, K. Inoue, Y. Kibe, Y. Kishimoto, M. Koga, A. Kozlov, Y. Minekawa, T. Mitsuui, K. Nakajima, K. Nakajima, K. Nakamura, M. Nakamura, K. Owada, I. Shimizu, Y. Shimizu, J. Shirai, F. Suekane, A. Suzuki, Y. Takemoto, K. Tamae, A. Terashima, H. Watanabe, E. Yonezawa, S. Yoshida, J. Busenitz, T. Classen, C. Grant, G. Keefer, D. S. Leonard, D. McKee, A. Piepke, M. P. Decowski, J. A. Detwiler, S. J. Freedman, B. K. Fujikawa, F. Gray, E. Guardincerri, L. Hsu, R. Kadel, C. Lendvai, K.-B. Luk, H. Murayama, T. O'Donnell, H. M. Steiner, L. A. Winslow, D. A. Dwyer, C. Jillings, C. Mauger, R. D. McKeown, P. Vogel, C. Zhang, B. E. Berger, C. E. Lane, J. Maricic, T. Miletic, M. Batygov, J. G. Learned, S. Matsuno, S. Pakvasa, J. Foster, G. A. Horton-Smith, A. Tang, S. Dazeley, K. E. Downum, G. Gratta, K. Tolich, W. Bugg, Y. Efremenko, Y. Kamyshev, O. Perevozchikov, H. J. Karwowski, D. M. Markoff, W. Tornow, K. M. Heeger, F. Piquemal, and J.-S. Ricol. Precision measurement of neutrino oscillation parameters with kamland. *Phys. Rev. Lett.*, 100:221803, Jun 2008.
- [2] Paul W. Allison, Joseph D. Sherman, and David B. Holtkamp. An emittance scanner for intense low-energy ion beams. *IEEE Transactions on Nuclear Science*, NS-30(4):2204–2206, August 1983.
- [3] S. Axani, D. Winklehner, J. Alonso, and J. M. Conrad. A high intensity H_2^+ multicusp ion source for the isotope decay-at-rest experiment, isodar. *Review of Scientific Instruments*, 87(02B704), 2016.
- [4] J. Buon. *Beam phase space and emittance*. LAL-RF-90-15-REV, LAL-RT-92-03, CAS-CERN Accelerator School: 5th General Accelerator Physics Course, pp.89-116. February 1992.
- [5] D. Campo, J. Alonso, W. Barletta, L. Bartoszek, A. Calanna, J. M. Conrad, M. Touns, and M. Shaevitz. High intensity compact cyclotron for isodar experiment. *Proceedings of Cyclotrons, Vancouver, Canada*, 2013.
- [6] A. J. T. Holmes. Theoretical and experimental study of space charge in intense ion beams. *Phys. Rev. A*, 19:389–407, Jan 1979.
- [7] K. Floettmann. Some basic features of the beam emittance. *Phys. Rev. Spec. Top.-Accel. Beams*, 6(034202), 2003.

- [8] Joachim Kopp, Pedro A. N. Machado, Michele Maltoni, and Thomas Schwetz. Sterile neutrino oscillations: the global picture. *Journal of High Energy Physics*, 2013(5):50, May 2013.
- [9] H. R. Kremers, J. P. M. Beijers, and S. Brandenburg. A pepper-pot emittance meter for low-energy heavy-ion beams. *Review of Scientific Instruments*, 84(025117), 2013.
- [10] T. Ludwig, K. Volk, W. Barth, and H. Klein. Quantization error of slit-grid emittance measurement devices. *Review of Scientific Instruments*, 65(1462), 1994.
- [11] M. C. Ross, J. T. Seeman, E. Bong, L. Hendrickson, D. McCormick, and L. Sanchez-Chopitea. Wire scanners for beam size and emittance measurements at the slc. *Stanford Linear Accelerator Center*, 1991.
- [12] M. P. Stockli, M. Leitner, D.P. Moehs, R. Keller, and R. F. Welton. Beam dumping ghost signals in electric sweep scanners. *AIP Conference Proceedings*, 763(145), 2005.
- [13] D. Winklehner, R. Hamm, J. Alonso, J.M. Conrad, and S. Axani. Preliminary design of a rfq direct injection scheme for the isodar high intensity H_2^+ cyclotron. *Review of Scientific Instruments*, 87(02B929), 2016.